

Structural and Morphological Transitions in Gold Nanorods: A Computer Simulation Study

Yanting Wang^{†,‡} and Christoph Dellago^{*,‡}

Department of Physics and Astronomy and Department of Chemistry, University of Rochester, Rochester, New York 14627

Received: February 21, 2003; In Final Form: June 4, 2003

When gold nanorods are exposed to low-energy laser pulses, they can undergo shape transitions at temperatures below melting. In the present study such transitions are reproduced in molecular dynamics simulations of gold nanorods consisting of 10^3 – 10^4 atoms. We find that the shape change is accompanied by a structural change. On the basis of the simulation results, a mechanism is suggested that explains the intermediate products and the internal defects of gold nanorods observed in laser heating experiments.

I. Introduction

The fundamental physical properties of nanocrystals, such as their electronic band structure and optical activity, can be drastically different from those of the corresponding bulk materials, mainly due to their large surface-to-volume ratio. But while size effects on the physical properties of nanoparticles are well-documented, less is known about the effects of shape and surface structure. Recently, however, research efforts of several groups have been directed toward investigating the dependence of optical and electronic properties on morphology.^{1,2} In particular, Chang et al.³ and Link et al.^{4,5} have explored the stability and structure of gold nanorods with various aspect ratios.

In these experiments, laser pulses are used to selectively heat gold nanorods essentially without affecting their environment. Although the energy delivered to the particles by the laser is selected to be under the threshold for complete melting, intermediate products with various shapes can be observed. In particular, bent, twisted, shorter and wider, and ϕ -shaped intermediates were found in these experiments.^{3,4} Furthermore, transmission electron microscopy revealed that point and planar internal defects appear inside gold nanorods as they undergo such shape transformations.⁵ Computer simulations can be used to clarify the mechanisms involved in these processes.

While gold nanorods have not been studied before with computer simulation, several of such studies have been carried out for gold nanospheres. Ercolessi et al.⁶ revealed that the melting temperature decreases when the gold cluster becomes smaller. This effect has been confirmed and investigated in detail by other workers.^{7–9} Liu et al.¹⁰ found that melting of nanometer-sized gold clusters occurs in three stages: surface disordering and reordering, surface melting, and overall melting.

In this paper we report on molecular dynamics simulations of the morphological and structural behavior of gold nanorods during continuous heating from 5 K to complete melting and compare our findings with experimental results. The simulated gold nanorods have the same aspect ratio as the experimental

rods but much smaller sizes of about 10^3 – 10^4 atoms. Our results indicate that gold nanorods melt in two stages: a shape transition at lower temperature in which the rods shrink to a shorter and wider shape precedes the melting transition to liquid nanospheres. Both surface and internal atoms undergo structural change during the whole process. Surface disordering and reordering were also observed. On the basis of these results, a mechanism for the shape transition of gold nanorods is suggested explaining the morphology of intermediate states^{3,4} and the internal defects found experimentally.⁵

II. Methods

Dimensions of the gold nanorods studied in the experiments by Link et al.^{4,5,11} vary from tens of nanometers to several micrometers containing more than 10^6 atoms. On today's computers ab initio simulation techniques providing an accurate description of interaction energies can be used to simulate systems consisting of up to hundreds of atoms.¹² However, gold nanorods with less than 1000 atoms are thermally unstable¹³ and can undergo several structural transitions upon heating.⁷ Such transitions do not occur in much larger rods, so that ab initio simulation results for gold nanorods with less than 1000 atoms cannot be directly compared to experimental results. Using less accurate but computationally less expensive model potentials, such as the embedded atom method,¹⁴ the Murrell–Mottram potential,¹⁵ the Lennard-Jones potential,¹⁶ the Morse potential,¹⁷ the many-body Gupta potential,¹⁸ or the many-body “glue” potential,¹⁹ one can extend the size of simulated gold nanorods to more than 10 thousand atoms. In this study, we have chosen the many-body “glue” potential, because it was found to yield an accurate description of bulk, defect, and surface properties of gold.¹⁹ In the “glue” model, the potential energy of a system of N atoms consists of a sum of pair potentials and a many-body “glue” energy:

$$V = \frac{1}{2} \sum_i \sum_{j \neq i} \phi(r_{ij}) + \sum_i U(n_i) \quad (1)$$

Here the sums run over all particles, $r_{ij} = |\mathbf{r}_i - \mathbf{r}_j|$ is the interatomic distance between atoms i and j , and $\phi(r)$ is the pair interaction energy. The many-body “glue” energy depends on

* Current address: Institute for Experimental Physics, University of Vienna, Boltzmannngasse 5, 1090 Vienna, Austria. E-mail: Christoph.Dellago@exp.univie.ac.at.

[†] Department of Physics and Astronomy.

[‡] Department of Chemistry.

the coordination numbers n_i defined for all atoms,

$$n_i = \sum_j \rho(r_{ij}) \quad (2)$$

where $\rho(r)$ is a short-ranged monotonically decreasing function of the interatomic distance r . Cutoffs of 3.9 Å for $\rho(r)$ and 3.7 Å for $\phi(r)$ are used and equations of motion are integrated with the velocity Verlet algorithm²⁰ with a time step of 4.3 fs.

As initial structure for our simulations we construct a nanorod with the geometry of the gold nanorods studied experimentally by Wang et al.¹¹ These rods have an aspect ratio of 3.0 and their sides consist of four large {100} and four large {110} facets oriented parallel to the rod axis. Each end has a {001} facet and four small {111} facets connecting the {110} and the {001} facets, and four small {110} facets connecting the {100} and the {001} facets. We carved out several gold nanorods with such surfaces from bulk gold with a pure fcc structure. All gold nanorods have the same aspect ratio of 3.0 but different sizes ranging from 1404 atoms to 11 076 atoms. To allow surface atoms to relax from fcc to a more favorable surface structure, the prepared pure fcc gold nanorods then went through a constant temperature molecular dynamics simulation at 5 K for 10^5 simulation steps (430 ps).

In the experiments with nanosecond laser pulses, the gold nanorods are heated continuously by the laser essentially without affecting their environment.⁴ To simulate this experimental procedure, the kinetic energy of the system is increased by a fixed amount at each molecular dynamics step by rescaling the velocities, so that the total energy increases linearly in time. The heating rate is 7×10^{12} K/s, which is below the rate of overheating in computer simulations.²¹

During the heating process the shape change of the gold nanorods was monitored by calculating the radius of gyration

$$r_g = \sqrt{\frac{1}{N} \sum_i [\mathbf{r}_i(t) - \mathbf{r}_c]^2} \quad (3)$$

where the sum runs over all particles and \mathbf{r}_c is the center of mass of the rod. The radius of gyration is large for rods with large aspect ratio and reaches its minimum value for spherical shape.

The time evolution of the nanorod's structure was followed by calculating bond order parameters.²² Bonds are defined as the vectors joining a pair of neighboring atoms with an interatomic distance of less than a certain cutoff radius (3.7 Å in our case). The general idea of bond order parameters is to capture the symmetry of bond orientations regardless of the bond lengths.²² The local order parameters associated with a bond \mathbf{r} are a set of numbers

$$Q_{lm}(\mathbf{r}) \equiv Y_{lm}(\theta(\mathbf{r}), \phi(\mathbf{r})) \quad (4)$$

where $\theta(\mathbf{r})$ and $\phi(\mathbf{r})$ are the polar and azimuthal angles of the bond with respect to an arbitrary reference frame and $Y_{lm}(\theta(\mathbf{r}), \phi(\mathbf{r}))$ are spherical harmonics. Only even- l spherical harmonics are considered so that they are invariant under inversion. Global bond order parameters can then be calculated by averaging $Q_{lm}(\mathbf{r})$ over all bonds:

$$\bar{Q}_{lm} \equiv \frac{1}{N_b} \sum_{\text{bonds}} Q_{lm}(\mathbf{r}) \quad (5)$$

where N_b is the number of bonds. To make the order parameters

TABLE 1: Bond Order Parameters for Face-Centered-Cubic (fcc), Hexagonal Close-Packed (hcp), Icosahedral, and Liquid Structures

geometry	Q_4	Q_6	\hat{W}_4	\hat{W}_6
fcc	0.190 94	0.574 52	-0.159 317	-0.013 161
hcp	0.097 22	0.484 76	0.134 097	-0.012 442
icosahedral	0	0.663 32	0	-0.169 754
liquid	0	0	0	0

invariant with respect to rotations of the reference frame, the second-order invariants are defined as

$$Q_l \equiv \sqrt{\frac{4\pi}{2l+1} \sum_{m=-l}^l |\bar{Q}_{lm}|^2} \quad (6)$$

and the third-order invariants are defined as

$$W_l \equiv \sum_{\substack{m_1, m_2, m_3 \\ m_1 + m_2 + m_3 = 0}} \begin{bmatrix} l & l & 1 \\ m_1 & m_2 & m_3 \end{bmatrix} \cdot \bar{Q}_{lm_1} \bar{Q}_{lm_2} \bar{Q}_{lm_3} \quad (7)$$

where the coefficients $[\dots]$ are the Wigner $3j$ symbols.²³ Furthermore, reduced order parameters almost independent of the precise definition of nearest neighbors can be defined:

$$\hat{W}_l \equiv \frac{W_l}{(\sum_m |Q_{lm}|^2)^{3/2}} \quad (8)$$

We used the four bond order parameters Q_4 , Q_6 , \hat{W}_4 , and \hat{W}_6 together to identify structures accurately. The values of these bond order parameters for fcc, hcp, icosahedral, and liquid structures are listed in Table 1.²⁴

Bond order parameters averaged over all bonds can be used to monitor global structural changes. Surface structures of nanomaterials, however, are often quite different from bulk structures. We therefore calculated bond order parameters for the internal atoms and the surface atoms separately. Here, an atom is defined to be part of the surface if there are less than 11 neighboring atoms in a spherical region with radius 3.7 Å around the atom.

Because the many-body ‘‘glue’’ potential uses cutoffs, a cell index method can be used to reduce the computational time.²⁰ In this method, the simulation box is divided into cubic cells with side lengths larger than the cutoff distance. When calculating energies and forces one considers only interactions between atoms within the same cell and the nearest 26 cells. This approach reduces the required computation time from order N^2 to order N . On a PC equipped with a 1.5 GHz AMD Athlon CPU and 1 GB of memory, 25 000 steps can be carried out per CPU-hour for a system of 2624 atoms propagating the system for about 100 ps.

III. Results

Since gold nanorods with less than 1000 atoms are unstable and simulations of more than 10 000 atoms are computationally too expensive for a thorough statistical analysis, we focus on gold nanorods with 1000 to 10 000 atoms in the present study. In particular, we carry out a detailed analysis of the shape transition for a 2624 atom nanorod. Results of a continuous heating run of such a gold nanorod with 2624 atoms and an aspect ratio of 3.0 are shown in Figures 1–3. Figure 1 shows four typical configurations of the rod at instantaneous temperatures of 5, 515, 1064, and 1468 K. (Here and throughout the rest of the paper the instantaneous temperature is defined as T

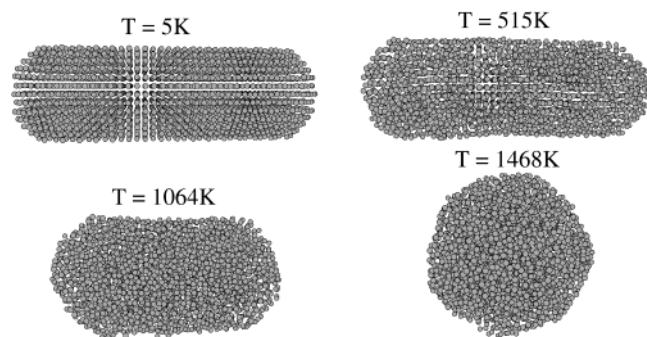


Figure 1. Snapshots from a continuous heating run of a gold nanorod with 2624 atoms at temperatures of 5, 515, 1064, and 1468 K.

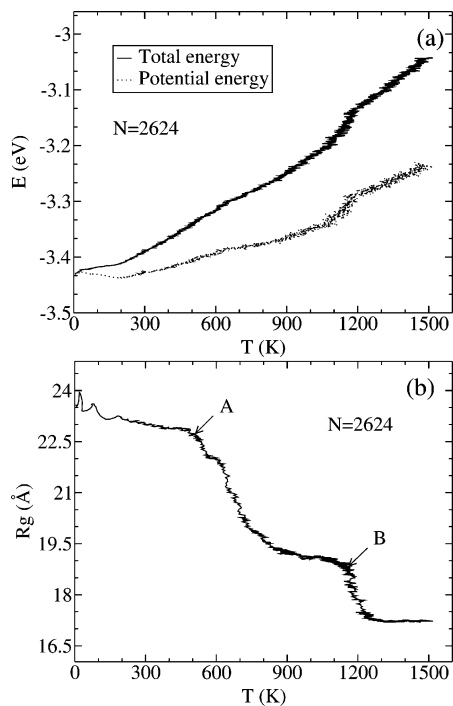


Figure 2. Temperature dependence of total and potential energy (a) and of the radius of gyration (b) for 2624 atoms during continuous heating with a heating rate of 7×10^{12} K/s. The letter A indicates the shape transition and the letter B indicates the onset of the melting transition.

$= 2K/3N$, where K is the instantaneous total kinetic energy and N is the number of particles.) During heating, the rod becomes slightly shorter and displays a less regular internal structure at 515 K. Then the rod becomes shorter and wider, acquiring an aspect ratio of 1.8 at 1064 K. Finally, the rod melts and forms a liquid sphere at 1468 K. The heating procedure from 5 to 1468 K takes about 420 ps.

The evolution of some system parameters during heating is depicted in Figures 2 and 3. The average total energy per atom versus instantaneous temperature is shown in Figure 2a. The slope of the E vs T curve changes significantly at about 200, 650, and 1100 K, indicating the occurrence of structural and morphological transitions. Figure 2b shows the temperature dependence of the radius of gyration of the gold nanorod. Before the temperature reaches 200 K, the radius of gyration oscillates due to a thermally excited long wavelength deformation. Then the radius of gyration decreases very slowly up to 500 K, after which the radius of gyration drops quickly, indicating that the rod collapses to a shorter and wider shape. It then decreases slowly up to 1140 K, when the melting begins and the shorter and wider rod collapses to a liquid sphere. After melting, the

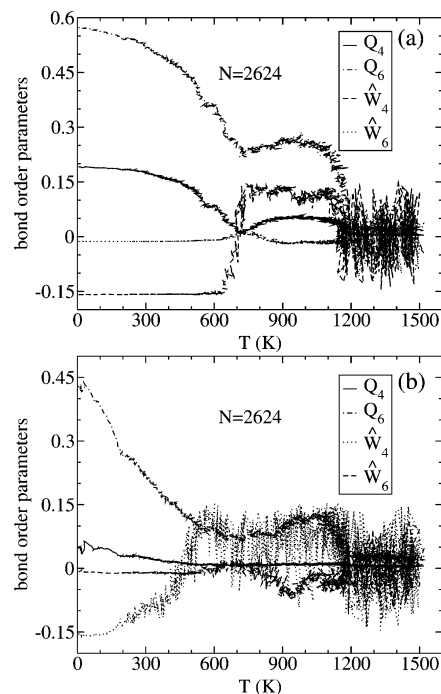


Figure 3. Temperature dependence of bond order parameters for the gold nanorod with 2624 atoms during continuous heating with a heating rate of 7×10^{12} K/s. (a) Average bond order parameters of internal atoms. (b) Average bond order parameters of surface atoms.

radius of gyration grows slowly and linearly with temperature, reflecting the thermal expansion of the liquid sphere. The globally averaged bond order parameters of the internal atoms are shown in Figure 3a. For temperatures below 650 K, the internal structure remains almost pure fcc. Then it changes quickly to an hcp-dominated structure. This hcp structure keeps nearly unchanged until the temperature reaches about 1140 K when the rod melts and the internal atoms acquire the structure of a liquid.

The above results indicate that continuous heating induces the gold nanorod to go through two distinct transformations: (1) a shape transition, in which the initial rod shrinks to the shorter and wider intermediate state with an aspect ratio of 1.8, and (2) the melting transition. The shape change is accompanied by a structural change.

The intermediate state appears to be stable on the simulation time scale for temperatures up to 1140 K. We have verified this (meta)stability by equilibrium simulation. Several configurations of the intermediate state at different temperatures were saved and then underwent constant energy MD simulations. Configurations at 743, 905, and 1033 K were stable for more than 400 ps. However, we cannot exclude that on experimental time scales, which are longer than the simulation time scales by many orders of magnitude, the intermediate state undergoes a transformation to a more spherical shape. Particularly at high temperatures curvature-driven surface diffusion provides a mechanism for such a transformation.²⁵ Whether this is indeed the case for the gold nanorods studied in the present paper remains a subject for future work.

The same simulation has been repeated with a three times higher heating rate (2.1×10^{13} K/s) and a three times lower heating rate (2.3×10^{12} K/s) (Figure 4). The intermediate-state phenomenon occurred in both simulations, but with some differences in the details. The most significant difference is that the internal structure of the intermediate state during slower heating returns to fcc-dominated after a short jump to hcp-

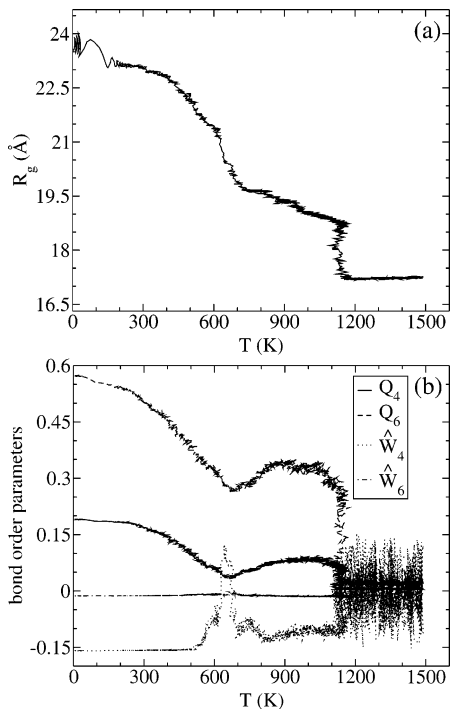


Figure 4. Temperature dependence of the radius of gyration (a) and the average bond order parameter for internal atoms (b) for 2624 atoms during continuous heating with a rate of 2.3×10^{12} K/s.

dominated rather than remaining hcp-dominated. Thus, the occurrence of a shape transition and the appearance of intermediate stable states appear to be qualitatively independent of the heating rate, but changes in the internal structure have a pronounced heating rate dependence.

Analogous computer simulations were also performed for gold nanorods with the same initial shape but different sizes of 1404, 2094, 3610, 4960, 5870, 7552, 9678, and 11 076 atoms. Essentially the same phenomenology was observed in all of the simulations, and the aspect ratio of the intermediate nanorods are all very close to 1.8. However, like in the case of different heating rates, the internal structures of the intermediate states range from hcp-dominated to fcc-dominated with different hcp/fcc ratios.

It is well-known that the melting temperature (T_m) of gold nanoclusters decreases with particle size. Our simulations indicate that the onset of the shape transition, T_s , has a strong size dependence as well. The instantaneous temperatures of the onsets of the shape and melting transitions, T_s and T_m , (corresponding to points A and B in Figure 2b) are shown in Figure 5. These temperatures were determined by visual inspection of the radius of gyration and bond order parameters versus temperature curves. Both the onset of the shape transition and of the melting transition increase with increasing sizes, but that of the melting transition increases more slowly. Thus, the shape transition temperature T_s approaches the melting transition temperature T_m with increasing system size. As a consequence, the shape transition is preempted by the melting transition and does not occur in large systems.

The aspect ratio of the intermediate state is 1.8 for all rods with different sizes but an identical initial aspect ratio of 3.0. This raises the question of whether an aspect ratio of 1.8 is universal for nanorods that underwent the shape transition. To answer this question, we have carried simulations of nanorods consisting of 3900, 3810, and 3686 particles with initial aspect ratios of 4.1, 5.0, and 6.0. Different aspect ratios of the intermediate state have been found as listed in Table 2,

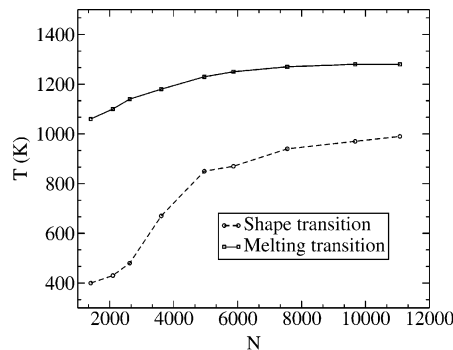


Figure 5. The temperatures of the onsets of the shape (T_s) and melting (T_m) transitions for gold nanorods of various sizes. These temperatures were determined by visual inspection of the R_g vs T curves as indicated by the arrows A and B in Figure 2b.

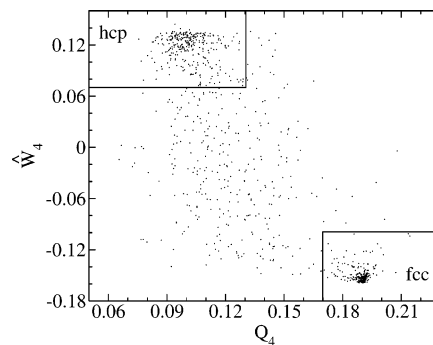


Figure 6. Order parameters Q_4 and \hat{W}_4 for internal atoms in a set of structures of the 2624-atom gold nanorod at 691 K. The atoms with $Q_4 < 0.13$ and $\hat{W}_4 > 0.07$ are considered atoms with local hcp structure. Those with $Q_4 > 0.17$ and $\hat{W}_4 < -0.10$ are atoms with local fcc structure.

TABLE 2: Aspect Ratios of the Intermediate States

no. of atoms	aspect ratio	
	initial	intermediate
3610	3.0	1.8
3900	4.1	2.5
3810	5.0	2.8
3686	6.0	4.2

suggesting that the shape (aspect ratio) is not sufficient to characterize the stable intermediate state completely.

To understand the transition mechanism during heating, fine structure analysis has been carried out for the gold nanorod with 2624 atoms. From the results of the globally averaged bond order parameters of the internal atoms we already know that the structure changes from fcc-dominated to hcp-dominated. We therefore concentrated on the analysis of fcc and hcp local structures and proceeded as follows. During heating, configurations were periodically saved and then minimized with respect to the total potential energy with the conjugate gradients method to eliminate thermal noise. For each minimized configuration, the number of nearest neighbors (with a cutoff of 3.7 \AA for the distance between two atoms) was determined for each atom. With very little exception, atoms with less than or equal to 10 neighbors lie on the surface of the cluster. For the atoms with 12 neighbors located in the interior of the cluster, local 13-atom bond order parameters have been calculated. Bond order parameters characteristic for the rod at 691 K are displayed in Figure 6. Here, Q_4 and \hat{W}_4 are used to distinguish fcc ($Q_4 > 0.17$ and $\hat{W}_4 < -0.10$) and hcp ($Q_4 < 0.13$ and $\hat{W}_4 > 0.07$) from other structures. Most atoms in the interior of the rod have fcc (bottom right corner) or hcp (top left corner) local structures.

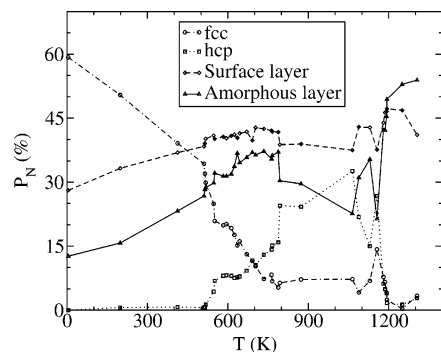


Figure 7. Fractions P_N of atoms in the surface layer, in the amorphous subsurface layer, and with fcc and hcp local structure versus temperature for the gold nanorod with 2624 atoms.

Other atoms, including the atoms with 11 neighbors or 13 or more neighbors, and atoms with 12 neighbors and without clear fcc or hcp signature, are distributed between the surface layer and the interior, forming an amorphous subsurface layer.

The fractions of atoms in the surface layer, in the amorphous subsurface layer, and in the bulk with fcc and hcp structure are shown in Figure 7 as a function of temperature. For temperatures below the shape transition temperature T_s , the population of hcp atoms remains very small, but the population of fcc atoms decreases linearly, due to the growth of the amorphous subsurface layer and the surface layer. At 510 K, the population of hcp atoms jumps to a higher value and keeps growing until another sudden increase at the end of the shape transition (800 K). In the intermediate state region, the population of fcc atoms stays almost unchanged and the fraction of hcp atoms grows, due to loss in the amorphous subsurface layer. After that, at about the onset of the melting transition (1140 K), the populations of both fcc and hcp atoms increase suddenly and then decrease quickly to near zero at 1250 K, when the nanorod is completely melted and the system is unstructured.

Configurations at different temperatures with atoms colored according to their local structures are shown in Figure 8. Below the shape transition the nanorod consists almost entirely of fcc atoms (yellow) with some atoms at the surface (gray) and some atoms in the subsurface layer (red). With increasing temperature the number of atoms in the amorphous layer grows, but the structure in the interior remains of fcc type. At a temperature of 517 K, there appear some hcp atoms along the $\{111\}$ facet. At 551 K, there are three groups of hcp atoms along $\{111\}$ facets at different directions across the fcc body. With increasing temperature, the number of hcp atoms in these three groups keeps growing. At the same time, the number of amorphous atoms increases (691 K). At 794 K, only three layers of fcc are left along the $\langle 001 \rangle$ direction at the top, the bottom, and middle of the hcp body and another layer along the $\langle 111 \rangle$ direction. It is remarkable that the surface of the nanorod at this temperature appears to be more ordered than at lower temperatures. At 1088 K there is only a middle layer of fcc along the $\langle 001 \rangle$ direction besides several solitary fcc atoms. At 1156 K, the number of fcc atoms increases again and the whole body is more ordered with an increasing number of hcp atoms. At a slightly higher temperature of $T = 1193$ K, melting sets in and the cluster becomes completely disordered and spherical at $T = 1305$ K. The two configurations between them ($T = 1180$ K and $T = 1192$ K in Figure 8) suggest that the melting propagates quickly from outside to inside of gold nanorods.

To gain a better understanding of the type of movement of the atoms leading to the shape change, we have determined a vector field shown in Figure 9. Each vector connects the position

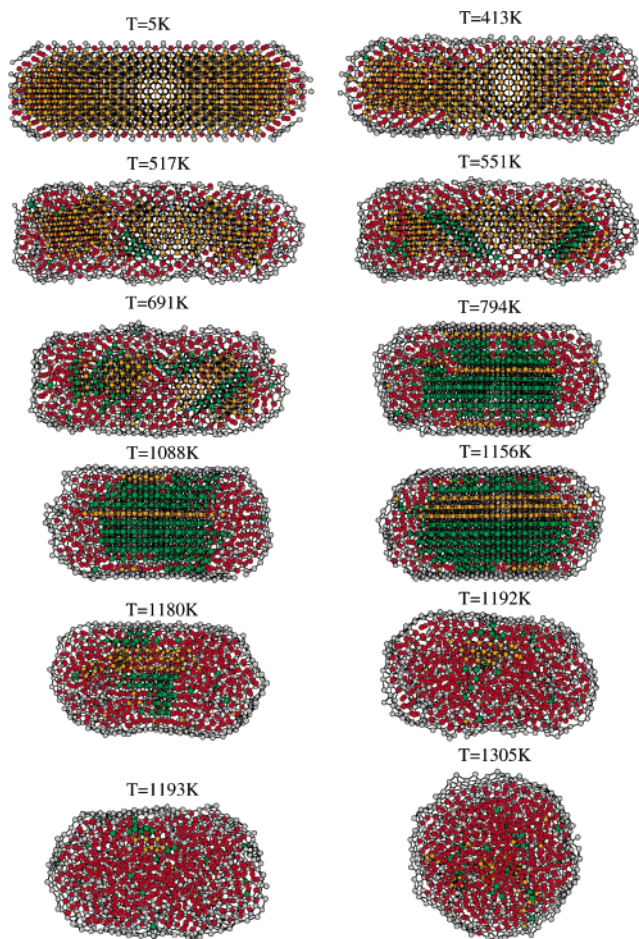


Figure 8. Configurations of the 2624-atom gold nanorod at different temperatures with atoms colored according to their local structure. The configurations have been cut into half to allow a better view of the internal structures. Surface atoms are gray, amorphous atoms are red, fcc atoms are yellow, and hcp atoms are green.

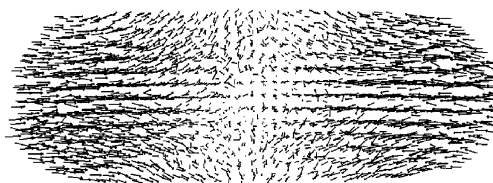


Figure 9. Motion of atoms during the transition. The initial configuration is at 511 K and the final configuration is at 794 K.

of an atom before the shape transition occurs (511 K) to the position of the same atom after completion of the shape transition (794 K). It is evident that surface atoms originating in the caps move toward the center and that surface atoms at the middle move radially away from the rod axis. While the center atoms move little, other internal atoms slide along the rod axis toward the center. This flow pattern is consistent with formation of the ϕ -shaped particles observed experimentally.^{3,4} However, we never detected such ϕ -shaped particles in our simulation. This might be due to the large size differences between our simulated nanoparticles and the ones studied in experiments.

Summarizing the above simulation results, two main transformations occur during continuous heating of gold nanorods: a shape transition and a melting transition. The shape change is accompanied by a structural change. The exact aspect ratio and the structure of the intermediate state depend on rod size, heating rate, and initial aspect ratio.

IV. Mechanism

From the simulation results discussed above the following picture for the mechanism of the morphological and structural transition emerges. Initially, at very low temperature (5 K in our case), the gold nanorod has a defect-free fcc body by construction. In such nanorods the surface atoms deviate slightly from the sites of an fcc structure (Figure 8, $T = 5$ K). Although the atoms immediately beneath the surface are close to their original fcc positions, they are classified as amorphous, because their neighboring surface atoms are displaced from their fcc sites.

During the heating toward the onset of the shape transition, the surface atoms display increasing deviations from their original positions. This not only leads to more irregularly arranged surface atoms but also helps the atoms beneath the surface to leave their original fcc positions to form the amorphous layer (Figure 8, $T = 511$ K). With increasing temperature, more and more atoms beneath the surface deviate from the local fcc structure so that the amorphous layer becomes thicker and the number of fcc atoms decreases (Figure 7).

It might be this build up of the amorphous layer that eventually drives the nanorod through the morphological transformation to a shorter rod with smaller surface area. When this happens, planes of atoms slide with respect to each other transforming fcc atoms into hcp atoms and vice versa. Such sliding events can happen independently at several different positions and in different directions (Figure 8, $T = 517$ K and $T = 551$ K). The resulting configurations are consistent with the experimentally observed point and planar defects inside the rods produced by laser heating.⁵

During the shape transition, the nanorod becomes shorter and wider. At the same time, the internal structure keeps changing from fcc-dominated to hcp-dominated (Figure 8, $T = 691$ K). In the case of $N = 2624$ atoms, the shape transition stops when the body is of almost pure hcp structure (Figure 8, $T = 794$ K). In clusters of different size, however, the shape transition produces intermediate states with fcc structure. The heating rate, the size, and the initial aspect ratio all affect the shape and structure of the intermediate state as well. On the nanosecond time scale of our simulations, the intermediate state is stable within a certain range of temperatures (Figure 8, $T = 1088$ K, the range is shorter in the cases of Figure 4) and corresponds to the shorter and wider gold nanorods found in experiments.^{3,4}

As the temperature keeps increasing, more amorphous atoms reorganize to be fcc or hcp, and more fcc layers transform from hcp (Figure 8, $T = 1156$ K). This observation is consistent with simulation result reported by Liu et al.¹⁰ that nanometer-sized gold particles experience surface disordering and reordering before melting. As the cluster reaches the melting temperature, both the surface and internal atoms become unstructured (Figure 8, $T = 1193$ K) and the cluster quickly collapses to a liquid nanosphere (Figure 8, $T = 1305$ K).

V. Conclusions

In agreement with experimental observations, our computer simulations indicate that, upon heating, gold nanorods undergo a morphological and structural transition before they eventually melt. During this transition the gold nanorods become shorter and wider. The shape transition is accompanied by an internal structural change from fcc-dominated to hcp-dominated. Further heating causes these intermediate, wider rods to melt and the rods become disordered, collapsing to spherical shape. Reordering of the internal atoms occurs shortly before melting. The mechanism we suggest for the shape transition explains the experimentally observed shorter and wider and ϕ -shaped intermediate particles as well as the internal point and planar defects. It is tempting to relate the shape transition to a surface instability caused by roughening or surface melting. Research in this direction is underway in our laboratory.

Acknowledgment. The authors thank Prof. Steve Teitel for useful discussions.

References and Notes

- (1) Alivisatos, A. P. *J. Phys. Chem.* **1996**, *100*, 13226.
- (2) Albe, V.; Jouanin, C.; Bertho, D. *J. Cryst. Growth* **1998**, *184/185*, 388.
- (3) Chang, S.; Shih, C.; Chen, C.; Lai, W.; Wang, C. R. *C. Langmuir* **1999**, *103*, 1165.
- (4) Link, S.; Burda, C.; Nikoobakht, B.; El-Sayed, M. A. *J. Phys. Chem. B* **2000**, *104*, 6152.
- (5) Link, S.; Wang, Z. L.; El-Sayed, M. A. *J. Phys. Chem. B* **2000**, *104*, 7867.
- (6) Ercolessi, F.; Andreoni, W.; Tosatti, E. *Phys. Rev. Lett.* **1991**, *66*, 911.
- (7) Lewis, L. J.; Jensen, P.; Barrat, J.-L. *Phys. Rev. B* **1997**, *56*, 2248.
- (8) Chushak, Y. G.; Bartell, L. S. *J. Phys. Chem. B* **2001**, *105*, 11605.
- (9) Shim, J.-H.; Lee, B.-J.; Cho, Y. W. *Surf. Sci.* **2002**, *512*, 262.
- (10) Liu, H. B.; Ascencio, J. A.; Perez-Alvarez, M.; Yacaman, M. J. *Surf. Sci.* **2001**, *491*, 88.
- (11) Wang, Z. L.; Mohamed, M. B.; Link, S.; El-Sayed, M. A. *Surf. Sci.* **1999**, *440*, L809.
- (12) Marx, D.; Hutter, J. *Ab initio molecular dynamics: Theory and implementation; Modern Methods and Algorithms of Quantum Chemistry*; Grotendorst, J., Ed.; Forschungszentrum Juelich, NIC Series, Vol. 1, 2000.
- (13) Yu, X.; Duxbury, P. M. *Phys. Rev. B* **1995**, *52*, 2102.
- (14) Foiles, S. M.; Baskes, M. I.; Daw, M. S. *Phys. Rev. B* **1986**, *33*, 7984.
- (15) Murrell, J. N.; Mottram, R. E. *Mol. Phys.* **1990**, *69*, 571.
- (16) Wales, D. J.; Doye, J. P. K. *J. Phys. Chem. A* **1997**, *101*, 5111.
- (17) Doye, J. P. K.; Wales, D. J. *J. Chem. Soc., Faraday Trans.* **1997**, *93*, 4233.
- (18) Garzon, I. L.; Jellinek, J. Z. *Phys. D* **1991**, *20*, 235.
- (19) Ercolessi, F.; Parrinello, M.; Tosatti, E. *Philos. Mag. A* **1988**, *58*, 213.
- (20) Allen, M. P.; Tildesley, D. J. *Computer Simulation of Liquids*; Clarendon Press: Oxford, 1987.
- (21) Liu, H. B.; Chen, K. Y.; An, G. Y.; Hu, Z. Q. *Philos. Mag. B* **1997**, *76*, 75.
- (22) Steinhardt, P. J.; Nelson, D. R.; Ronchetti, M. *Phys. Rev. B* **1983**, *28*, 784.
- (23) Landau, L. D.; Lifshitz, F. M. *Quantum Mechanics*; Pergamon: New York, 1965.
- (24) van Duijneveldt, J. S.; Frenkel, D. *J. Chem. Phys.* **1992**, *96*, 4655.
- (25) Combe, N.; Jensen P.; Pimpinelli A. *Phys. Rev. Lett.* **2000**, *85*, 110.